A computational model of electrically coupled, intrinsically distinct pacemaker neurons

Cristina Soto-Trevi[(1)], **Pascale Rabbah**[(2)], **Eve Marder**[(3)], **Farzan Nadim**[(1,2)]

[(1)] Department of Mathematical Sciences and
Center for Applied Mathematics and Statistics
New Jersey Institute of Technology, Newark, NJ 07102

[(2)] Dept of Biological Sciences, Rutgers University-Newark

[(3)] Volen Center and Biology Dept, Brandeis University

CAMS Report 0405-07, Fall 2004

Center for Applied Mathematics and Statistics

NJIT

January 6, 2005

A computational model of electrically coupled, intrinsically distinct pacemaker neurons

Cristina Soto-Treviño
Volen Center, Brandeis University, Waltham MA 02454 and Department of Mathematical Sciences, New Jersey Institute of Technology, NJ 07102.
cristina@stg.rutgers.edu

Pascale Rabbah
Department of Biological Sciences, Rutgers University, Newark, NJ 07102.
pascale@stg.rutgers.edu

Eve Marder
Volen Center and Biology Department, Brandeis University, Waltham, MA 02454. marder@brandeis.edu

Farzan Nadim
Department of Mathematical Sciences, New Jersey Institute of Technology and Department of Biological Sciences, Rutgers University, Newark, NJ 07102.
farzan@njit.edu

Abbreviated title: Model of electrically coupled pacemaker neurons

Corresponding Author: Farzan Nadim, Department of Biological Sciences, Rutgers University, 135 Smith Hall, Newark, NJ 07102. Phone: (973) 353-1541, Fax: (973) 353-1007

Key words: gap junctions, pyloric rhythm, stomatogastric ganglion, lobster, oscillation

Abstract

Electrical coupling between neurons with similar properties is often studied. Nonetheless, the role of electrical coupling between neurons with widely different intrinsic properties also occurs, but is less well-understood. Inspired by the pacemaker group of the crustacean pyloric network, we developed a multi-compartment, conductance-based model of a small network of intrinsically distinct, electrically coupled neurons. In the pyloric network, a small intrinsically bursting neuron, through gap-junctions, drives two larger, tonically spiking neurons to reliably burst in-phase with it. Each model neuron has two compartments, one responsible for spike-generation and the other for producing a slow, large amplitude oscillation. We illustrate how these compartments interact, and determine the dynamics of the model neurons. Our model captures the dynamic oscillation range measured from the isolated and coupled biological neurons. At the network level, we explore the range of coupling strengths for which synchronous bursting oscillations are possible. The spatial segregation of ionic currents significantly enhances the ability of the two neurons to burst synchronously, and the oscillation range of the model pacemaker network depends not only on the strength of the electrical synapse but also on the identity of the neuron receiving inputs. We also compare the activity of the electrically coupled, distinct neurons with that of a network of coupled identical bursting neurons. For small to moderate coupling strengths, the network of identical elements, when receiving asymmetrical inputs, can have a smaller dynamic range of oscillation than that of its constituent neurons in isolation.

Introduction

Cells that are electrically coupled through gap junctions are found in numerous biological tissues, including nervous systems of both vertebrates and invertebrates (Bennett 1997; Dermietzel and Spray 1993). The common role of electrical coupling among neurons is believed to be synchronization of their activities (Jefferys 1995; Perez Velazquez and Carlen 2000) although theoretical studies show that electrical coupling can lead to more complex network activity (Chow and Kopell 2000; Sherman and Rinzel 1992). When the neurons involved are intrinsically distinct, the behavior of an electrically coupled two-cell network can be fairly unintuitive (Medvedev and Kopell 2001; Wilson and Callaway 2000). A passive neuron electrically coupled to an oscillatory neuron can have a non-monotonic effect on the oscillatory cell frequency as the coupling strength is increased (Kepler et al. 1990). Electrical coupling between an oscillatory and a bistable neuron can result in a wide variety of behaviors, again depending on their intrinsic properties and the coupling strength (Kopell et al. 1998).

The rhythmically active pyloric network of the crustacean stomatogastric ganglion (STG) is driven by a pacemaker kernel consisting of one Anterior Burster (AB) neuron and two Pyloric Dilator (PD) neurons that are electrically coupled. The AB neuron is a small neuron which, when isolated from all local network interactions, produces rhythmic bursts of action potentials. The PD neurons are larger than the AB neuron and in isolation they fire tonically. Rhythmic bursting cannot be typically induced in the PD neurons by externally injected current (Eisen and Marder 1984; Miller and Selverston 1982). These neurons differ also in the neurotransmitters they use (Marder and Eisen 1984b), their response to neuromodulators, and pre- and postsynaptic targets (Marder and Eisen 1984a). In the intact network, the AB-PD group reliably produces in-phase bursts in a wide frequency range that can be altered by current injection (Ayali and Harris-Warrick 1999; Eisen and Marder 1984; Hooper 1997; Miller and Selverston 1982).

We developed a model of an electrically coupled AB-PD pair. To take into account the distinct intrinsic and dynamic properties of these neurons we used current

measurements from STG cultured neurons of the spiny lobster *Panulirus interruptus* (Turrigiano et al. 1995) as a starting point. To tune the model to capture the dynamic activity of the biological pacemaker neurons, we used experimental data from the individual isolated neurons or the isolated pacemaker group under the two conditions in which they are usually experimentally studied; namely, in the absence and presence of the descending neuromodulatory inputs to the STG.

We use this model to illustrate at the single neuron level, behaviors that arise from coupling compartments which in isolation are capable of producing very different oscillations. At the network level we explore the coupling ranges for which an intrinsically bursting neuron drives a tonic spiking neuron to burst synchronously with it, and the effect of the compartmental structure on their ability to synchronize. We conclude by asking how the dynamical repertoire of an intrinsically bursting neuron is affected when it is electrically coupled to an identical neuron or to an intrinsically distinct one.

Methods

Experiments

Adult male and female spiny lobsters (*Panulirus interruptus*), weighing 400-800 g, were purchased from Don Tomlinson Fisheries (San Diego, CA) and kept in artificial seawater tanks at 12-15 ºC until use. Prior to dissection, the animals were covered in ice for approximately 30 minutes. Standard methods (Harris-Warrick 1992; Selverston et al. 1976) were used to isolate the stomatogastric nervous system (including the STG, the oesophageal (OG) and the paired commissural (CoG) ganglia) which was then pinned down in a Sylgard-coated Petri dish. The preparations were superfused with normal saline, 18ºC, pH 7.35 containing (in mM): 12.8 KCl, 479 NaCl, 13.7 $CaCl_2$, 10.0 $MgSO_4$, 3.9 $NaSO_4$, 11.2 Trizma base, and 5.1 Maleic acid.

The STG was desheathed to allow penetration of the cell bodies. Glass microelectrodes pulled using a Flaming-Brown micropipette puller (Sutter Instruments, Novato, CA) were filled with 0.6 M K_2SO_4 and 0.02 M KCl (resistance 15-23 MΩ) for neuron identification and current injections or backfilled with 5-10% lucifer yellow (in dH_2O) backfilled with 1 M LiCl (resistance 30-50 MΩ) for photoinactivation.. Identification of the neurons was achieved by matching their intracellular recordings to extracellular recordings on motor nerves (Selverston et al. 1976).

Upon identification, the neurons were isolated by photoinactivating all neurons that establish synaptic connections onto them. Namely, for AB isolation, the two PD and the ventricular dilator (VD) neurons were inactivated while for PD isolation, the AB, the VD and the lateral pyloric (LP) neurons were inactivated. In order to isolate the AB-PD group, the VD and LP neurons were inactivated. The complete photoinactivation procedure is outlined in Eisen and Marder (1984), Hooper and Marder (1987) and Miller and Selverston (1982).

Once isolated, the AB neuron was impaled with two electrodes, one for injecting current and one for recording voltage in current clamp. The current-injection protocol was carried out using an Axoclamp 2B amplifier (Axon Instruments, Union City, CA).

Single square pulses (duration 60 s) were injected into the AB neuron with various DC current levels to shift the baseline membrane potential ±70 mV from rest. For isolated PD neuron experiments, both PD neurons were impaled with two electrodes and current was injected into both neurons simultaneously using the same protocol as above. For isolated AB-PD unit experiments, the AB neuron and one PD neuron were impaled with two electrodes each. Descending neuromodulatory inputs to the STG were reversibly blocked by building a Vaseline well around the desheathed stomatogastric nerve which was filled with 1 M sucrose and 10^{-6} M Tetrodotoxin (TTX; Biotium, Hayward, CA).

A Digidata 1332A board was used for data acquisition and current injection with pClamp 9 software (Axon Instruments, Union City, CA). The acquired data were saved as individual binary files and were analyzed either with the readscope software (http://stg.rutgers.edu/software/software.htm) developed in the Nadim laboratory or with scripts on a Linux platform.

Simulations

Each neuron was modeled with two compartments, one representing the soma, primary neurite and dendrites (S/N) and the other representing the axon (A). The A compartments are responsible for the production of axon potentials. In each compartment the membrane potential V obeyed the current conservation equation

$$C\frac{dV}{dt} = I_{ext} - I_{\text{int}} - I_{coup},$$

where C is the membrane capacitance, I_{ext} is the externally injected current, I_{int} the sum of intrinsic and modulatory currents and I_{coup} is the sum of the axial current (I_{axial}) from the adjacent compartment and (in the case of the S/N compartment) the gap-junctional current (I_{gap}).

The intrinsic and modulatory currents were based primarily on experimental data from *P. interruptus* STG cultured neurons (Turrigiano et al. 1995). These currents are described as a product of a maximal conductance g_i, activation m_i and inactivation h_i

variables, and a driving force ($V_i - E_i$), where E_i is the reversal potential that corresponds to the particular ion *i*:

$$I_i = g_i\, m_i^{p_i}\, h_i^{q_i}\, (V - E_i).$$

The exponents p_i and q_i take integer values between 0 and 4, depending on the current type. The behavior of the activation and inactivation variables is described by:

$$\tau_m(V)\frac{dm}{dt} = m_\infty(V) - m,$$
$$\tau_h(V)\frac{dh}{dt} = h_\infty(V) - h$$

where m_∞ and h_∞ represent the steady-state values, and τ_m and τ_h the respective time constants. The dependence on voltage and intracellular Ca^{2+} concentration ($[Ca^{2+}]$) of each of these functions is given in Table 1. The values of maximal conductances g_i are given in Table 2.

In the S/N compartments, $[Ca^{2+}]$ is governed by

$$\tau_{Ca}\frac{d[Ca^{2+}]}{dt} = -FI_{Ca} - [Ca^{2+}] + C_o,$$

where τ_{Ca} is the Ca^{2+} buffering time constant, C_o is the background intracellular Ca^{2+} concentration and the factor *F* translates the total Ca^{2+} current I_{Ca} (in nA) into an intracellular concentration. The values of τ_{Ca}, *F* and C_o used in this model are given in Table 2.

The reversal potential E_{Ca} for the calcium currents was computed using the intracellular calcium concentration from the Nernst equation, assuming an extracellular concentration of 13 mM (Buchholtz et al. 1992). All other reversal potentials were constant and are given in Table 2.

In the case of the model AB neuron, the presence of neuromodulatory inputs was modeled by adding a fast, non-inactivating, voltage-gated, inward current referred to as

the modulatory proctolin current I_{proc} (Golowasch et al. 1992; Swensen and Marder 2000). The voltage-dependence and related parameters of the proctolin current are described in Tables 1 and 2. Because, in *P. interruptus*, proctolin has no effect on the biological PD neuron (Hooper and Marder 1987), we modeled the presence of neuromodulatory inputs in the PD neuron not by adding I_{proc}, but as an increase in the maximal conductance of the Ca^{2+} currents (Table 2) which have been shown to be targets of modulation in this neuron (Johnson et al. 2003).

The mathematical description for the axial currents I_{axial} and the gap-junctional currents I_{gap} is the same. For each model neuron the axial current in the S/N compartment $I_{axial_{S/N}}$ is the product of an axial conductance and the difference of the membrane potential in the A and S/N compartments:

$$I_{axial_{S/N}} = g_{axial}(V_{S/N} - V_A).$$

Similarly, I_{gap} is the product of a gap-junctional conductance and the membrane voltage difference of the two S/N compartments:

$$I_{gap_{PD}} = g_{gap}(V_{S/N_{PD}} - V_{S/N_{AB}}).$$

Coupling currents in coupled compartments were symmetrical: $I_{axial_{S/N}} = -I_{axial_A}$ and $I_{gap_{PD}} = -I_{gap_{AB}}$.

The simulations were performed on a PC with the Linux platform using the *network* software developed in the Nadim laboratory. We used a 4th order Runge-Kutta numerical integration method with time steps of 0.05 and 0.01 ms.

Results

The behavior of the AB-PD network in response to current injection

In order to tune the qualitative behavior of the model to match that of the biological network, we used a dynamic perturbation of the biological AB-PD oscillator after synaptic isolation from other STG neurons. By injecting different values of constant DC current into the AB or PD neurons, the activity of these neurons changed from quiescent to bursting to tonic firing in different conditions. We first examined the activity of these neurons with the neuromodulatory inputs to the STG intact.

A comparison between the behavior of the biological neurons (left traces) and the model (right traces) is shown in Figure 1. In each panel, the gray background illustrates the traces with 0 current injection, and depolarizing and hyperpolarizing DC current was injected in increasing amounts. In all cases shown, the model network mimicked the activity of the biological neurons.

In the intact network (Fig. 1A), with 0 current injection, the AB and PD neurons showed in-phase rhythmic bursting activity. Hyperpolarization of the AB neuron caused the bursting cycle to slow down and the amplitude of the oscillations to decrease. With sufficient hyperpolarization, the neurons became quiescent. Depolarization of the AB neuron increased the oscillation frequency and decreased its amplitude. The electrically coupled model AB-PD neurons showed behavior similar to the biological neurons (Fig. 1A).

The isolated biological AB neuron always showed bursting oscillations and showed a similar response with the oscillation frequency increasing as the depolarization was increased (Fig. 1B, left). However, in contrast with the intact AB-PD network, the amplitude of oscillations consistently decreased as a function of injected current. The isolated AB neuron typically did not exhibit pure tonic firing with large injected DC current. Instead it produced high-frequency and low-amplitude bursts of 2-3 action potentials (Fig. 1B, left top trace). The isolated model AB neuron showed behavior similar to that of the biological neuron.

In contrast to the isolated AB neuron, isolated biological PD neurons typically showed only tonic spiking activity (Fig. 1C, left middle trace) whose frequency increased with injected current. Injection of negative current silenced this activity. In some cases (N = 2 of 5), the isolated PD neuron showed weak rhythmic bursting activity that turned into tonic spiking with positive current injection (data not shown). Again, the model PD neuron (Fig. 1C, right) showed behavior similar to that of the biological neuron.

Removing the neuromodulatory inputs to the STG drastically changes the activity of the AB-PD network (Bal et al. 1988; Miller and Selverston 1982; Selverston and Miller 1980). The activity of the AB-PD kernel in the absence of neuromodulatory inputs is shown in Fig. 2. Without current injection the biological AB-PD neurons were typically quiescent (Fig. 2, bottom left panel, gray) or weakly tonically active (not shown). Injection of positive DC current caused these neurons to produce weak bursting oscillations with 1-3 spikes per burst. The oscillation frequency increased and its amplitude decreased with injected current. Removal of the modulatory currents in the model AB and PD neurons (Fig. 2, right) resulted in a model AB-PD kernel that showed behavior similar to that of the biological coupled AB-PD neurons.

In the absence of neuromodulatory inputs, the isolated biological AB neuron was silent (N = 4 of 5. In one preparation however, small amplitude oscillations were recorded in the isolated AB neuron.) Positive current injection produced very weak bursts with 1-2 spikes per burst (N = 5, data not shown). The isolated PD neuron showed tonic activity very similar to its activity in the presence of neuromodulatory inputs (N = 3, data not shown).

Figure 3A shows a qualitative comparison of the waveforms of the AB neuron when coupled to the PD neurons (thin trace) and after isolation from the PD neurons (thick trace). The amplitude and number of spikes/burst were measured in 5 preparations (5 cycles each), and consistent with the data shown in Figure 3A, the spike amplitude per burst increased by an average of 142% (SD 64%) while the number of

spikes per burst decreased by an average of 45% (SD 11%). Figure 3B shows a similar comparison of the waveforms for the model AB neuron, in isolation (thick trace) and when coupled to the model PD neuron (thin trace). The model AB neuron showed a decrease in burst amplitude and increase in period when coupled to the model PD neuron, as well as an increase in the burst duration and the number of spikes per burst. These changes were consistent with the experimental results. These data show that the amplitude of the AB neuron slow wave is significantly decreased by its coupling to the PD neurons

Understanding the network model behavior as a function of its components

The AB-PD neuron model described in the previous section has a number of properties. We now wish to describe how these properties contribute to the behavior of the model, and use these to make some more general statements about networks in which non-identical neurons are electrically coupled.

a) The two compartments of the model neurons:

Our model is based loosely on voltage-clamp descriptions of the currents recorded from cultured lobster STG neurons (Turrigiano et al. 1995). Figure 4A shows a schematic representation of the segregation of the currents in the two compartments in the model neurons. The currents responsible for action potential generation were separated from those responsible for the generation of slow oscillations (~1 Hz; see Fig. 4B) for the following reasons: 1) Pyloric neurons produce slow-wave voltage oscillations in the absence of action potentials (Raper 1979), 2) Under some modulatory conditions (such as high frequency stimulation of the inferior ventricular nerve, a modulatory nerve that connects the brain to the stomatogastric nervous system), the PD neuron is able to produce long, slow bursts (Eisen and Marder 1984; Miller and Selverston 1982).

In each model neuron, the action potentials were generated in the axon (A) compartment by fast sodium I_{Na} and delayed-rectifier potassium I_{Kd} currents with Hudgkin-Huxley type dynamics. The compartments labeled as S/N represent the soma and primary neurite. The A compartment was excitable, but in isolation from the S/N compartment remained quiescent (Fig. 4B). In the S/N compartment, the intrinsic

outward currents were a delayed-rectifier I_{Kd}, a calcium-dependent I_{KCa} and a transient I_A potassium current. The inward currents consisted of a transient I_{CaT} and a persistent I_{CaS} calcium current, a persistent sodium current I_{NaP} and a hyperpolarization-activated inward current I_h. To model the effect of descending modulatory inputs, a voltage-gated inward current (such as the one activated by the neuropeptide proctolin) I_{proc} was added to the S/N compartment of the model AB neuron (Fig. 4A) (Blitz et al. 1999; Hooper and Marder 1987; Marder et al. 1986). In the case of the isolated biological PD neuron in *P. interruptus*, however, proctolin has been reported to show no noticeable effect (Hooper and Marder 1987). Thus, the presence of modulatory inputs in the PD neuron was modeled as a slight increase in the conductances of the two Ca^{2+} currents (Johnson et al. 2003). Together with the leak current I_L, the currents in the S/N compartments generated large amplitude (~35mV) slow oscillations with a frequency of about 1 Hz (Fig. 4B).

Figure 4C shows the results of coupling each of the S/N compartments with its respective A compartment, with axial conductances as in Table 2. In the model AB neuron, the electrical interaction between the excitable A compartment and the intrinsically oscillatory S/N compartment produced intrinsic bursting activity (Fig. 4C, top panel). In contrast, in the case of the PD model neuron (Fig. 4C, bottom panel), the electrical interaction between the excitable A compartment and the intrinsically oscillatory S/N compartment produced tonic spiking activity (see below). The electrical synapse between the AB and the PD neurons was modeled by coupling the two S/N compartments (gap-junction conductances as in Table 2). This coupling caused the PD neuron to burst in-phase with the AB neuron (Fig. 4D), as seen in the biological network.

b) The roles of axial and gap-junction conductances

Figures 5A and B show the isolated AB and isolated PD model neurons, respectively, as the axial conductance between their two compartments was increased from top to bottom. The gray background shows the "reference" model with parameters as in Tables 1 and 2. When the axial conductance between the S/N and A compartments of the isolated AB neuron was weak, the activity of the neuron was very similar to its isolated S/N compartment (Fig. 5A, top trace). As the axial conductance was increased,

both the spike amplitude and the number of spikes per burst consistently increased. In contrast, the AB neuron burst amplitude and period behaved non-monotonically: they initially decreased and then increased. Increasing the axial conductance value to 1.3 μS served to merge the S/N and A compartments of the model AB neuron and effectively turn it into a one-compartment bursting neuron (Fig. 5A, bottom trace). Note that, in this case, the amplitude of the action potentials was considerably larger. (This increase occurred as a fairly sudden transition as the axial conductance was increased from 0.4 to 0.5 μS; not shown). Irrespective of the strength of the axial coupling, the AB neuron always remained an intrinsic burster, although as the coupling was increased more than 0.4 μS the waveform of the biological AB neuron was lost..

In contrast, as the axial conductance between the two compartments of the model isolated PD neuron was increased (Fig. 5B), there was a range of coupling values for which PD was not able to produce intrinsic bursting oscillations. For small coupling values, small to medium-size spikes rode on top of the slow wave oscillation of the S/N compartment. As the axial conductance increased, the coupling current had a hyperpolarizing effect on the burst phase of the S/N compartment which eventually prevented the S/N compartment from producing slow oscillations. The S/N compartment, however, could still induce spiking in the A compartment and, therefore, the neuron spiked tonically. Both irregular bursting and tonic spiking could be obtained for the same conductance strength, as is shown in the second and third traces of Fig. 5B. Further increasing the axial conductance served to increase the spike frequency (and amplitude) and to subsequently cause enough calcium ion accumulation to activate I_{KCa} and thus restore bursting. For large axial coupling (in excess of 20 μS), the model was effectively a single-compartment burster with overshooting spikes (Fig. 5B, bottom trace).

Figure 5C shows the behavior of the model AB-PD pacemaker group as the strength of the electrical coupling between the two neurons was increased from top to bottom by varying the gap-junctional conductance values. The gray background shows the “reference” model with parameters as in Tables 1 and 2. For very small coupling, the AB neuron produced irregular bursting and, although the PD neuron produced long

small-amplitude bursts, it was not able to fire in phase with the AB neuron (Fig. 5C, top panel). As the coupling strength increased, both model neurons produced regular bursts, but the PD neuron burst started slightly after and lasted longer than the AB neuron burst. In this case, the spikes of the two neurons occurred out of phase (Fig. 5C, second trace). Further increasing the coupling strength caused the slow wave oscillation of the neurons to become better aligned, the number of spikes per burst to increase, and the spikes, though not completely synchronized, to occur almost in phase (Fig. 5C, superimposed traces in middle panel). In order for the waveforms of the AB and PD neurons to be almost indistinguishable from each other, the coupling strength needed to be further increased, as shown in the bottom trace in Fig. 5C. Remarkably, most gap-junctional conductance values used resulted in synchronous oscillations of the model AB and PD neurons. In the following subsection, we show that this need not be the case if the model neurons involved are one-compartment neurons.

c) Two-compartment models provide a more robust bursting mechanism for the pacemaker network

Thus far, we have used our two-compartment per neuron model to show that it is possible for an intrinsically bursting neuron to drive a tonically spiking neuron to oscillate in synchrony with it for a wide range of coupling strengths. We now address the question of whether it is possible to obtain similar results with one-compartment model neurons. To answer this question, we built several AB-PD networks, and assayed the network oscillations as the gap junction strength was varied (Fig. 6). We used two distinct versions of the model AB and PD neurons. These were either the "reference" model neurons (AB and PD) or slightly modified versions of these neurons (AB and PD). The S/N compartment of the PD neuron was intrinsically oscillatory, as in Fig. 4B, whereas that of PD lacked I_{KCa} and thus PD had no intrinsic ability to oscillate (and was quiescent). The AB neuron had a smaller transient calcium current I_{CaT} (g_{CaT} = 42 μS) than the AB neuron, which decreased the slow oscillation amplitude. This reduction in g_{CaT} was done so that the one-compartment (see below) AB neuron would have a slow wave oscillation similar to that of the two-compartment reference AB neuron.

We then addressed the significance of compartmentalization by comparing the one- and two-compartment model neurons. The one-compartment neurons were obtained by increasing (100-fold or more) the axial conductance between the A and S/N compartments, thus effectively collapsing the two compartments. (These are shown schematically in Fig. 6A with the whole region between the two compartments shaded.) The networks were divided into four cases (I-IV) and in each case, we compared the coupling of the AB (or AB) neuron to either the PD or the PD neuron, resulting in a total of 8 networks (Fig. 6A). The behavior of the "reference" AB-PD network is highlighted in the gray box in Fig. 6A. The case of the two compartment AB was similar to case I and it is not shown.

To measure the electrical "load" that the PD neuron placed on the AB neuron, the burst amplitudes of the coupled and isolated AB neurons (see Fig. 6A) were compared for the networks that produced synchronous bursting. When the network output was tonic, the ratio of the burst amplitudes was set to zero. The ratios as a function of the gap-junction conductance were plotted for Cases I-IV (Figs. 6B and 6C). These ratios were compared to the range (0.65-0.85) calculated from the biological AB neuron as in the experiment shown in Fig. 3A.

In Case I, we used the "reference" two-compartment model AB neuron and coupled it to either a one-compartment model PD (Fig. 6A, left column) or model PD neuron (Fig. 6A, right column). In contrast to PD, PD was able to burst in synchrony with the AB neuron for all coupling strengths (Fig. 6A, Case I). However, the burst amplitude of the AB neuron increased as the coupling strength was increased irrespective of whether it was coupled to PD or PD (Fig. 6A, Case I). When AB was coupled to PD, the range of gap-junction conductances for which the burst amplitude ratio remained within the biological range (0.65-0.85) was ~1-2 μS (see Fig. 6A, Case I, left column, fourth panel from top, g_{gap}= ~1.6 μS and Fig. 6B, orange circles). For large coupling conductances (g_{gap}>2 μS), this AB-PD network output was very similar to that of the two-compartment AB neuron with large axial coupling (compare Fig. 6A, case I, left column, bottom panel to Fig. 5A, bottom panel). When the AB neuron was coupled to the PD

neuron (Fig. 6A, Case I, right column), the network behavior progressed from tonic spiking for small to moderate coupling conductances to large amplitude bursting for large coupling conductances (g_{gap}>2 μS; Fig. 6A, Case I, right panel and Fig. 6C, orange circles).

In Case II, we replaced the two-compartment AB neuron with the one compartment AB neuron which had a similar slow-wave amplitude of oscillations (compare the top voltage traces in Fig. 6A, Cases I and II). When the model AB neuron was coupled to the one-compartment model PD neuron, this network was able to produce bursting oscillations for only moderate to large coupling strengths (Fig. 6A, Case II, left column). However, the burst amplitude ratios of the coupled to the uncoupled AB neuron calculated as the gap-junctional conductance was increased did not fall within the biological range (Fig. 6B, green triangles), suggesting that the burst amplitudes of AB were either too small or too large. Coupling the AB neuron to the one-compartment PD neuron produced only tonic spiking behavior for all but large coupling strengths, in which case the burst amplitude of AB was again too large (Fig. 6C, green triangles).

In Case III, the burst amplitude of the one-compartment model AB neuron was considerably larger (84%) than that of the "reference" AB neuron. Even with this larger-amplitude oscillation in the model AB neuron, however, when it was coupled to the one-compartment model PD (Fig. 6B, blue inverted triangles) or PD (Fig. 6C. blue inverted triangles) neuron, the range of gap-junction conductances for which the burst amplitude ratio of the AB neuron was adequate was very small. As in Cases I and II, with large coupling strengths, the network behavior was very similar to that of the two-compartment AB neuron with a large axial conductance (compare the bottom panel of Fig. 5A to the bottom panels of the first 6 columns in Fig. 6A). From these results, we suggest that a one-compartment model PD (and PD) neuron behaves as an additional "axon" on the AB oscillator.

In contrast, as shown in Case IV, the two-compartment per neuron networks were able to function similar to the biological pacemaker for a wider range of coupling

strengths (Fig. 6A). The burst amplitude ratio of the coupled to the uncoupled model AB neuron remained in the biological range for a much wider range of gap-junction conductances than in any of the previous cases (see Figs. 6B and 6C, black squares). However, similar to Cases I-III, large coupling strengths increased the burst amplitude of the AB neuron to values that were beyond the biological range. The burst durations in Case IV remained stable for all coupling strengths (21-38 ms) as opposed to the networks with one-compartment neurons, in which the burst durations shortened for large coupling strengths (10-15 ms). A similar shortening of the burst duration occurred in the isolated model AB neuron when the axial coupling between its two compartments was large (see Fig. 5A, bottom trace). This is consistent with our earlier suggestion, based on burst amplitudes, that the one-compartment model PD (and PD) neuron behaves as an additional "axon" on the AB oscillator.

Functional consequences of electrically coupling two identical and two distinct neurons

So far we showed that compartmentalization provides a reliable mechanism for the model neurons to produce in-phase bursts when they are electrically coupled. We then proceeded to examine the functional consequences of coupling identical or different neurons on bursting oscillations. We did this by comparing a model AB-AB network to the reference model AB-PD network and to the isolated AB neuron. We assayed differences among these models by measuring the range of oscillation periods each model produced in response to DC current injection (Fig. 7). For each value of the gap-junction conductance, increasingly larger amounts of hyper- or depolarizing DC current were injected in the S/N compartment of one of the coupled neurons until the network became silent or produced irregular bursts or tonic activity.

The two limits of the oscillation period range produced by the AB-AB network when DC current was applied to one AB neuron are plotted in Fig. 7A. In the absence of current injection (dashed line) for all coupling strengths the bursting oscillation produced by each of the coupled AB neurons was indistinguishable from each other and from those of the isolated model AB neuron. However, the asymmetry introduced by injecting DC

current into one of the two identical AB neurons when they were weakly coupled did not allow them to completely synchronize but instead caused them to become phase-locked, as shown in the inset of Fig. 7A (g_{gap}=0.1 μS). The AB neuron that received the hyperpolarizing DC input (Fig. 7A, inset, lighter red trace) bursted after its coupled twin neuron. Note that when the two identical AB neurons are completely in phase, $I_{gap} = 0$ (not shown). In contrast, the slightly out of phase oscillation of the coupled AB neurons results in a non-zero I_{gap}, thus producing a load on the oscillation of each neuron. As a result, for weak coupling strengths (g_{gap}<0.3 μS), the period range of the AB-AB network was actually smaller than that of the isolated AB neuron (period range of isolated AB marked with gray area). As the gap junction conductance was increased, however, the period range of the AB-AB network approached that of the isolated AB neuron until they became identical for g_{gap} > 15 μS (not shown). For all coupling strengths shown, the hyperpolarizing DC current injection that caused the coupled AB neuron to become quiescent was 100% more than the current for the isolated AB neuron. In contrast, the minimum depolarizing DC current that caused the coupled AB neuron to produce tonic spiking, compared to the current for the isolated AB neuron, increased from 31% (at g_{gap}=0.1 μS) to 315% (at g_{gap}=3 μS) as the gap junction conductance was increased.

Fig. 7B shows that with small to moderate gap junction conductances, the AB-PD network could oscillate with longer periods (up to 18%) than the isolated AB neuron. The inset in Fig. 7B shows simultaneous voltage traces of weakly coupled (g_{gap}=0.1 μS) model AB and PD neurons when the AB neuron was hyperpolarized (note that the two neurons are more in phase here than those shown in the other two insets of Fig. 7). For larger coupling strength (g_{gap}=3 μS), the longest period that the coupled AB-PD network produced was 26% smaller than that produced by the isolated AB neuron (Fig. 7B) and decreased up to 46% for even larger coupling (g_{gap}=100 μS , not shown). For the range of coupling strengths shown in Fig. 7B, the hyperpolarizing DC current necessary to silence the coupled AB-PD network was 15% more than the current for the isolated AB neuron, while the depolarizing DC current necessary for transition to tonic spiking was never more than 50% of the current for the isolated AB neuron. Taken together, these results suggest that, for moderate coupling strength, the presence of the PD neuron broadens the

period range of the AB-PD network to encompass larger periods (up to 5 s) as DC current is injected into the AB neuron, while it continues to buffer the activity of the AB neuron from hyperpolarizing inputs.

When DC current was injected into the PD neuron, the period range of the AB-PD network was smaller than that of the isolated AB neuron for all coupling strengths (Fig. 7C). The inset of Fig. 7C (g_{gap}=0.1 μS) illustrates that for small coupling strengths, the injection of hyperpolarizing current into the model PD neuron was more effective in disrupting synchronous bursting of the AB-PD network (the AB neuron fired slightly earlier than the PD neuron) than current injection into the model AB neuron (compare with inset of Fig. 7B). For small to moderate coupling strengths current injection into the PD neuron prevented the network from oscillating as slowly as it would if current were injected into the AB. As the gap junction conductance was increased (Figs. 7B and 7C), the difference in oscillation range as a consequence of current injection into either the AB or PD neuron slowly diminished, and eventually the oscillation ranges became identical (g_{gap}=100 μS, not shown). For the range of gap junction conductances shown in Fig. 7C, the amount of hyperpolarizing DC current (injected in the PD neuron) that caused the AB-PD network to become silent was 15% to 35% more than the current for the isolated AB neuron. Thus, similar to the case shown in Fig. 7B, the presence of the model PD neuron buffered the AB-PD network from hyperpolarizing inputs. However, in this case, the model AB-PD network was able to tolerate only 10% to 24% of the amount of depolarizing current that the isolated AB neuron would before transitioning to tonic spiking. These values should be contrasted with the much larger depolarizing current necessary to eliminate bursting in the AB-AB network (Fig. 7A), despite the fact that the PD neuron had a lower input resistance than the AB neuron (14.8 MΩ for AB and 6.9 MΩ for PD; see also legend of Fig. 4).

The role of ionic currents in the model and the action of neuromodulators

The biological AB and PD neurons are differentially modulated by a variety of different amines and neuropeptides (Ayali and Harris-Warrick 1999; Flamm and Harris-Warrick 1986; Hooper and Marder 1987; Marder and Eisen 1984a). To provide some

insight into function of differential modulation of two electrically coupled but distinct neurons, we examined the time course of activity of the inward (Fig. 8, top panels) and outward (Fig. 8, bottom panels) currents when descending neuromodulatory inputs were present. Variations of the leak current I_L (plotted separately in the middle panels of Fig. 8) allow for a comparison of the time course of the membrane potential in all cases, since the membrane potential is linearly related to I_L ($V_m = E_L + I_L/g_L$).

The membrane potential oscillation in the S/N compartment of the model AB neuron was obtained by a balance between the inward and outward currents (Fig. 8A). During the slow initial rise of the membrane potential, the inward currents barely dominated the outward currents until I_{proc} and I_{CaS} strongly activated to produce a more rapid rise of the membrane potential. This rise was followed by a rapid increase in the outward current I_{Kd} with smaller contributions from I_A and I_{KCa}. In the most depolarized phase, the outward and inward currents were in balance. At this time, the calcium-activated outward current I_{KCa} increased, first gradually and then rapidly, to produce a fall in the membrane potential of the neuron, and the cycle repeated. In the absence of I_{KCa}, the membrane potential remained in a depolarized steady-state (not shown). For the generation of this large slow wave voltage oscillation, I_{NaP}, I_h and I_A were not necessary: the slow wave was still produced in their absence (not shown). The oscillation period of about 1 s was set mainly by the activation and inactivation time constants of the transient calcium current I_{CaT} and was modulated by the maximal conductances of the leak current I_L and the outward currents I_{Kd} and I_{KCa}.

When the S/N compartment of the AB neuron was coupled to the A compartment (Fig. 8B), an initial slow rise of the membrane potential that was similar to the uncoupled case occurred until the membrane potential was large enough for the axial current to induce the generation of action potentials in the axon. Thus began the active or spiking phase which subsequently ended by the activation of I_{KCa}. An increase of 33% in the maximal conductance of I_{KCa} decreased both the number of spikes per burst (by 1) and the burst duration, while a decrease of 50% in the maximal conductance produced a longer burst duration with one extra spike per burst (not shown). The way in which the

transition from bursting to tonic spiking took place as constant depolarizing current was injected into the S/N compartment of the AB neuron depended on the amount of I_{KCa}. Increasing g_{KCa} shortened the burst duration (with no applied current) and maintained bursting with larger amounts of current injection. With smaller g_{KCa}, depolarizing current injection produced a transition to the tonic spiking regime more easily. This was a smooth transition where no irregular bursting or spiking was seen (not shown).

Recall that the neuromodulatory actions on the AB neuron were modeled by adding the ionic current I_{proc}. When g_{proc} in the model was set to 0 to mimic the removal of neuromodulatory actions on the AB neuron, the large voltage oscillation in the S/N compartment of the AB neuron was lost (not shown). In this case, a small voltage oscillation could be obtained by injecting a small constant depolarizing current. This small oscillation was enough to trigger a single spike per cycle and the model neuron produced small amplitude bursts, with only one spike per burst. The amplitude of the oscillation and the number of spikes per burst could be increased by increasing g_{CaT} (not shown).

The currents involved in the generation of the large amplitude voltage oscillation of the S/N compartment of the isolated PD neuron are shown in Fig. 8. There were several differences between these oscillations and those of the S/N compartment of the model AB neuron. First, in the S/N compartment of the PD neuron, the persistent calcium current I_{CaS} was more prominent than the transient I_{CaT}. Second, the calcium-dependent potassium current I_{KCa} was smaller. Third, the large oscillation as a single stable sate depended on the presence of the hyperpolarization activated current I_h: in its absence there was bistability between a quiescent state and the large oscillation. The oscillation still persisted, however, in the absence of I_{NaP} and I_A. Figure 8D shows the role of the intrinsic currents in the S/N compartment of the PD neuron when it is coupled to its A compartment. In this case, I_h provided enough background depolarization to allow the A compartment to fire continuously. In turn, the axial current from the A compartment to the S/N compartment had a hyperpolarizing effect that prevented it from continuing to produce large amplitude oscillations and, hence, the two-compartment neuron spiked

tonically. Note that the leak current was now entirely outward, since the spiking occurred above the leak reversal potential (-60 mV), and that I_{KCa} played a very small role. In this case, the smaller I_{CaT} to I_{CaS} ratio and smaller I_{KCa} (compared to the model AB neuron S/N compartment) were essential to produce the correct output for the isolated PD neuron. If either g_{CaT} was increased by more than 15%, or g_{KCa} was increased by 80% the two-compartment PD neuron became an intrinsic burster (not shown). However, if both g_{CaT} and g_{CaS} were increased by 20%, the two-compartment coupled PD neuron remained tonically spiking. An increase of more than 50% of g_{NaP} could also turn this spiking neuron into a bursting one, while an increase of more than 50% in g_A caused it to become quiescent (not shown).

We modeled the removal of the neuromodulatory inputs onto the PD neuron by a slight decrease in the maximal conductance of the calcium currents. The persistent current (g_{CaS}) was decreased by 10%, which served to decrease the spiking frequency by removing some of the background depolarization provided by this current (see Fig. 8D, top panel). The transient current (g_{CaT}) was decreased by 66.6%. This change had the effect of turning the PD neuron into a quiescent cell that spiked tonically with a small depolarizing current injection (not shown). The roles of the intrinsic currents in this case were very similar to those shown in Fig. 8D and hence are not shown. It is interesting to note that the PD model neuron could be built and tuned (by changing g_{CaT} to 20.5 μS and g_{proc} to 35 μS from those shown in Table 2) to have a neuromodulatory current I_{proc}, as in the AB neuron, and yet produce a similar activity as the model PD neuron described above (not shown). In this case, the removal of I_{proc} from the PD neuron would have effects that are similar to those obtained by decreasing the calcium currents (data not shown).

Figure 9 shows the currents in the S/N compartments of the model AB and PD neurons when these two compartments were electrically coupled, mimicking the gap-junction in the biological network. The electrical coupling current allowed the PD neuron to produce slow, bursting oscillations in phase with the AB neuron. In turn, the coupling current into the S/N compartment of the AB neuron affected the waveform of the AB

neuron by diminishing its burst amplitude, lengthening both the burst and the silent phases and thereby increasing its period (see also Fig. 3B). The gap-junctional current in the AB neuron (Fig. 9, left column, third trace from top) was mostly hyperpolarizing during the silent phase and also (at least on average) during the initial part of the burst. This was consistent with the decrease in amplitude of the AB neuron burst, as well as the lengthening of the silent phase. The lengthening of the AB neuron burst phase was mainly due to the depolarizing effect from the gap-junctional current later in the burst. The roles of the intrinsic currents of the coupled AB neuron (Fig. 9 left column) are very similar to those of the isolated AB neuron (Fig. 8B). The most noticeable difference between the intrinsic currents of the coupled PD neuron (Fig. 9, right column) and those of its isolated S/N compartment (Fig. 8C) was that the leak current I_L in the case of the coupled PD is completely hyperpolarizing, since the S/N compartment oscillation was above its leak reversal potential. This difference, however, was not significant since by decreasing the maximal conductance of the leak current by 31%, the membrane potential oscillation in the coupled PD neuron also hyperpolarized below its leak reversal potential (not shown). In both the isolated S/N compartment of the model PD and the coupled PD neurons, an increase of 24% in the maximal conductance of the leak current I_L had the effect of increasing the oscillation period; the increase was of 27% in the isolated S/N compartment of the PD neuron, and of 42% in the coupled PD neuron (not shown). The amplitude of the oscillation, however, was basically not affected by an increase of 24% in the maximal conductance of I_L in the case of the isolated S/N compartment of the PD neuron, while it did decrease in the case of the coupled PD neuron by 2 mV (not shown).

Discussion

The common intuition on the role of gap-junctions is that they synchronize the activity of similar neurons. Several modeling and analytical studies have addressed the role that electrical coupling plays in neuronal systems and these studies indicate a more complex role. For example, in networks of identical integrate-and-fire spiking neurons, different activity patterns of the network such as synchronous, asynchronous and phase-locked modes depend on the spike shape, amplitude and frequency as well as the strength of the coupling between the neurons (Chow and Kopell 2000). Electrical coupling can extend the parameter range over which initially uncoupled model neurons were able to burst (Komendantov et al. 2004; Sherman and Rinzel 1992). When heterogeneity is introduced in diffusely-coupled bursting neurons synchronous behavior can be destabilized (De Vries et al. 1998). However, the right combination of heterogeneous conductances with appropriate coupling strengths in electrically coupled non-oscillator model neurons can produce synchronous oscillatory behavior (Manor et al. 1997).

Chains of strongly diffusively coupled oscillators, each with a distinct intrinsic frequency, can display very long transients before reaching a stationary periodic state in which the frequency is the mean of the individual oscillator frequencies (Medvedev et al. 2003; Wilson and Callaway 2000). Combinations of electrical coupling and chemical synapses could produce yet more complexity in the network output. In a network of electrically coupled neurons that reciprocally inhibit each other, the generation and stabilization of bursting behavior was attributed to the electrical coupling between them (Skinner et al. 1999).

In this study we set out to explore the consequences of electrical coupling between two intrinsically distinct neurons. In particular, we focused on electrical coupling between a bursting neuron to a larger, tonic spiking, neuron inspired by the pacemaker network of the lobster pyloric CPG. We developed a two-compartment per neuron network of the pacemaker, and used the model to illustrate a variety of neuron and network behaviors arising from electrically coupling very different oscillators.

The AB-PD model and the biological AB-PD pacemaker

We have built a model of the lobster pyloric pacemaker network, consisting of the strongly electrically coupled AB and PD neurons, in which the two neurons are modeled as separate cells taking into account their distinct intrinsic dynamics. Our model captures the qualitative dynamic behavior of the actual network: a) It has a wide frequency range, b) the burst amplitude decreases with increasing frequency, c) as the frequency increases, the number of spikes per burst decrease, d) there is a transition to tonic spiking in which irregular small bursting and irregular spiking occurs, and e) with sufficiently high depolarizing current the network produces tonic spiking. Although the evolution from bursting to tonic spiking is qualitatively similar to that of the biological network, our model shows higher sensitivity to hyperpolarizing than to depolarizing current injection compared to the biological neurons. This difference is probably due to the specific voltage dependence properties of the currents we used. Our model does not include low-threshold regenerative inward currents since no such current has yet been characterized in the biological AB and PD neurons. The calcium currents have half-maximum potential values at somewhat depolarized values whereas the calcium-dependent potassium currents are activated at fairly low voltage values. As more measurements of ionic currents from the biological AB and PD neurons become available, the model can be refined to reflect better the intrinsic properties of these pacemaker neurons.

Both neurons were modeled using the same intrinsic currents. The only major differences were the time constants for the inactivation of I_{CaT} and the steady-state activation slope of the calcium-dependent potassium current I_{KCa} (see Table 1). These differences acted to prevent the model PD neuron from bursting in isolation by having a slower inactivation of I_{CaT} and a less abrupt activation of I_{KCa}. Whether or not the biological AB and PD neurons express all of the same currents is not known. It is quite possible, however, that these two neurons express different ratios of calcium channel types (Johnson et al. 2003) and our modeling results would predict this. In our model, it was necessary that the AB and PD neurons have different I_{CaT} to I_{CaS} conductance ratios, with more of the non-inactivating I_{CaS} in the PD neuron.

The AB-PD modeling strategy

In each model neuron, action-potential generation was segregated from other intrinsic currents. In the case of the intrinsically bursting AB neuron, the separation of currents allowed the model neuron to burst intrinsically for basically all axial coupling strengths. As the axial coupling strength between its two compartments was varied the oscillation frequency first increased and then decreased. This is in agreement with one of the two behaviors described in Kepler et al. (1990), in which the effect of electrically coupling a hyperpolarized, passive cell to an intrinsic, relaxation oscillator are described. The behavior of the model PD neuron was a bit more complicated but also more interesting: its compartments exhibited bursting behavior for both small and large axial conductances, but for an intermediate range of conductance values exhibited tonic spiking behavior or bistability between bursting and tonic spiking. Thus, depending on the strength of the axial coupling, the intrinsic dynamics of one compartment dominated the behavior at the neuron level. Although the actual mathematical mechanism for these behavioral transitions still needs to be analyzed, the overall non-monotonic behavior of the bursting frequency in these two compartments (first decreasing and then increasing as the axial coupling strength increased) is similar to some of those described in Kopell et al. (1998) for the effect of electrically coupling a bistable element to a relaxation oscillator.

At the network level, we have illustrated that both a one- and a two-compartment intrinsic bursting neuron, when very strongly electrically coupled to a tonic spiking neuron, can drive the spiking neuron to burst synchronously with it. However, this was not necessarily the case when the coupling was small to moderate. Instead, the spiking neuron was able to dominate the network dynamics and prevent the oscillator from bursting when one-compartment model neurons were used. Segregating the currents responsible for action-potential generation from other intrinsic currents allowed the electrical coupling to provide a very robust mechanism for producing synchronous bursting oscillations: the range of coupling strengths for which synchronous bursting was possible widened considerably to include small to intermediate coupling strengths. This could potentially have significant consequences for electrically coupled networks of non-

electrotonically-compact neurons in that the spatial structure and the location of the gap junctions may determine their ability to synchronize.

Asymmetric perturbations in networks of electrically coupled neurons

The synaptic and modulatory inputs received by electrically coupled neurons are often asymmetrical and this asymmetry may have functional consequences for the network behavior (Blatow et al. 2003; Galarreta and Hestrin 1999; Gibson et al. 1999; Johnson et al. 1994; Landisman et al. 2002; Marder and Eisen 1984a). We showed that the period range of oscillations of two identical, electrically coupled bursting neurons receiving asymmetric inputs, if the coupling is weak to moderate, can be smaller than that of the isolated neurons. On the other hand, the dynamic range of inputs to an isolated, bursting neuron may be expanded when it is electrically coupled to a distinct neuron. Our results suggest that in the coupled network, the AB and PD neurons may play distinct roles in the regulation of longer cycle periods, whereas their role is similar for shorter cycle periods: the coupled network cannot produce bursting oscillations with periods as short as those of the isolated AB neuron. These results also suggest that the presence of the PD neuron may simultaneously buffer the AB neuron oscillation from hyperpolarizing inputs while making the AB-PD network more sensitive to depolarizing inputs.

An experimental example of asymmetric effects of synaptic inputs to a network occurs in the biological AB-PD pacemaker. High-frequency stimulation of the inferior ventricular nerve (*ivn*), which synaptically affects these electrically coupled neurons, results in an increase in the AB-PD network burst amplitude and frequency. Stimulation of *ivn* produces asymmetrical responses from each neuron in isolation: the burst frequency of the AB neuron decreases and the PD neuron undergoes a long, slow depolarization (Marder and Eisen 1984a; Miller and Selverston 1982). It is this long depolarization on the PD neuron that is thought to be responsible for the network response. The effect of *ivn* stimulation on the PD neuron, characterized in Sigvardt and Mulloney (1982), consists of a fast excitation, a slower inhibition followed by a long-lasting depolarization. The total synaptic current could be seen as an additional current

contributing to the axial current from the A compartment into the S/N compartment of the PD. This contribution would amount to an effective change in the maximal conductance of the axial current, and we have seen that such a change, if sufficiently large in either direction, can turn the model tonic spiking PD neuron into a bursting neuron.

The examples presented throughout this work help illustrate that neuromodulation that acts at any of the different network levels, be it by modifying intrinsic properties, coupling conductances and/or synaptic inputs, could change the effective compartmental structure of the network, and thus significantly modify the network behavior.

Grants

This work was supported by National Institute of Mental Health Grant MH60605 (FN). CST was supported by National Science Foundation Grant IBN0090250.

TABLE 1: Voltage and calcium dependence for the steady-state activation *m* and inactivation *h* of the currents. The function was used for both neurons unless indicated.

	m,*h*	x_∞	τ_x (ms)
I_{Na^+}	m^3	$\frac{1}{1+\exp(-(V+24.7)/5.29)}$	$1.32-\frac{1.26}{1+\exp(-(V+120)/25)}$
	h	$\frac{1}{1+\exp((V+48.9)/5.18)}$	$\left(\frac{0.67}{1+\exp(-(V+62.9)/10)}\right)*\left(1.5+\frac{1}{1+\exp((V+34.9)/3.6)}\right)$
I_{CaT}	m^3	$\frac{1}{1+\exp(-(V+25)/7.2)}$	$55-\frac{49.5}{1+\exp(-(V+58)/17)}$
	h	$\frac{1}{1+\exp((V+36)/7)}$	AB: $87.5-\frac{75}{1+\exp(-(V+50)/16.9)}$ PD: $350-\frac{300}{1+\exp(-(V+50)/16.9)}$
I_{CaS}	m^3	$\frac{1}{1+\exp(-(V+22)/8.5)}$	$16-\frac{13.1}{1+\exp(-(V+25.1)/26.4)}$
I_{Nap}	m^3	$\frac{1}{1+\exp(-(V+26.8)/8.2)}$	$19.8-\frac{10.7}{1+\exp(-(V+26.5)/8.6)}$
	h	$\frac{1}{1+\exp((V+48.5)/4.8)}$	$666-\frac{379}{1+\exp(-(V+33.6)/11.7)}$
I_h	m	$\frac{1}{1+\exp((V+70)/6)}$	$272+\frac{1499}{1+\exp(-(V+42.2)/8.73)}$
I_K	m^4	$\frac{1}{1+\exp(-(V+14.2)/11.8)}$	$7.2-\frac{6.4}{1+\exp(-(V+28.3)/8.73)}$
I_{KCa}	m^4	AB: $\left(\frac{[Ca]}{[Ca]+30}\right)\frac{1}{1+\exp(-(V+51)/4)}$ PD: $\left(\frac{[Ca]}{[Ca]+30}\right)\frac{1}{1+\exp(-(V+51)/8)}$	$90.3-\frac{75.9}{1+\exp(-(V+46)/22.7)}$
I_A	m^3 (AB) m^4 (PD)	$\frac{1}{1+\exp(-(V+27)/8.7)}$	$11.6-\frac{10.4}{1+\exp(-(V+32.9)/15.2)}$
	h	$\frac{1}{1+\exp((V+56.9)/4.9)}$	$38.6-\frac{29.2}{1+\exp(-(V+38.9)/26.5)}$
I_{proc}	m	$\frac{1}{1+\exp(-(V+12)/3.05)}$	0.5

TABLE 2: Parameter values of the model. The numbers in parentheses denote the absence of modulatory inputs.

		AB		PD	
		g_i (μS)	E_i (mV)	g_i (μS)	E_i (mV)
AXON	I_{Na}	300	50	1110	50
	I_K	52.5	-80	150	-80
	I_L	0.0018	-60	0.00081	-55
	C	1.5 nF		6.0 nF	
SOMA	I_{CaT}	55.2		22.5 (10)	
	I_{CaS}	9		60 (54)	
	I_{Nap}	2.7	50	4.38	50
	I_h	0.054	-20	0.219	-20
	I_K	1890	-80	1576.8	-80
	I_{KCa}	6000	-80	251.85	-80
	I_A	200	-80	39.42	-80
	Iproc	570 (0)	0		
	I_L	0.045	-50	0.105	-55
	C	9.0 nF		12.0 nF	
	$[Ca]$	τ_{ca} = 303 ms, F=0.418 μ M/nA, C_o=0.5 μ M		τ_{ca} = 300 ms, F=0.515 μ M/nA, C_o=0.5 μ M	
	I_{coup}	g_{axial}= 0.3 μ S, $g_{gap=}$ 0.75 μ S		g_{axial} =1.1 μ S, $g_{gap=}$ 0.75 μ S	

References

Ayali A and Harris-Warrick RM. Monoamine control of the pacemaker kernel and cycle frequency in the lobster pyloric network. *J Neurosci* 19: 6712-6722, 1999.

Bal T, Nagy F, and Moulins M. The pyloric central pattern generator in crustacea: A set of conditional neuronal oscillators. *J Comp Physiol* 163: 715-727, 1988.

Bennett MV. Gap junctions as electrical synapses. *J Neurocytol* 26: 349-366, 1997.

Blatow M, Rozov A, Katona I, Hormuzdi SG, Meyer AH, Whittington MA, Caputi A, and Monyer H. A Novel Network of Multipolar Bursting Interneurons Generates Theta Frequency Oscillations in Neocortex. *Neuron* 38: 805-817, 2003.

Blitz DM, Christie AE, Coleman MJ, Norris BJ, Marder E, and Nusbaum MP. Different proctolin neurons elicit distinct motor patterns from a multifunctional neuronal network. *J Neurosci* 19: 5449-5463., 1999.

Buchholtz F, Golowasch J, Epstein IR, and Marder E. Mathematical model of an identified stomatogastric ganglion neuron. *J Neurophysiol* 67: 332-340, 1992.

Chow CC and Kopell N. Dynamics of spiking neurons with electrical coupling. *Neural Comput* 12: 1643-1678, 2000.

De Vries G, Sherman A, and Zhu HR. Diffusively coupled bursters: Effects of cell heterogeneity. *B Math Biol* 60: 1167-1200, 1998.

Dermietzel R and Spray DC. Gap junctions in the brain: where, what type, how many and why? *Trends Neurosci* 16: 186-192, 1993.

Eisen JS and Marder E. A mechanism for production of phase shifts in a pattern generator. *J Neurophysiol* 51: 1375-1393, 1984.

Flamm RE and Harris-Warrick RM. Aminergic modulation in lobster stomatogastric ganglion. II. Target neurons of dopamine, octopamine, and serotonin within the pyloric circuit. *J Neurophysiol* 55: 866-881, 1986.

Galarreta M and Hestrin S. A network of fast-spiking cells in the neocortex connected by electrical synapses. *Nature* 402: 72-75, 1999.

Gibson JR, Beierlein M, and Connors BW. Two networks of electrically coupled inhibitory neurons in neocortex. *Nature* 402: 75-79, 1999.

Golowasch J, Buchholtz F, Epstein IR, and Marder E. Contribution of individual ionic currents to activity of a model stomatogastric ganglion neuron. *J Neurophysiol* 67: 341-349, 1992.

Harris-Warrick RM. *Dynamic biological networks : the stomatogastric nervous system*. Cambridge, Mass.: MIT Press, 1992.

Hooper SL. Phase maintenance in the pyloric pattern of the lobster (Panulirus interruptus) stomatogastric ganglion. *J Comput Neurosci* 4: 191-205, 1997.

Hooper SL and Marder E. Modulation of the lobster pyloric rhythm by the peptide proctolin. *J Neurosci* 7: 2097-2112, 1987.

Jefferys JG. Nonsynaptic modulation of neuronal activity in the brain: electric currents and extracellular ions. *Physiol Rev* 75: 689-723, 1995.

Johnson BR, Kloppenburg P, and Harris-Warrick RM. Dopamine modulation of calcium currents in pyloric neurons of the lobster stomatogastric ganglion. *J Neurophysiol* 90: 631-643, 2003.

Johnson BR, Peck JH, and Harris-Warrick RM. Differential modulation of chemical and electrical components of mixed synapses in the lobster stomatogastric ganglion. *J Comp Physiol [A]* 175: 233-249, 1994.

Kepler TB, Marder E, and Abbott LF. The effect of electrical coupling on the frequency of model neuronal oscillators. *Science* 248: 83-85, 1990.

Komendantov AO, Komendantova OG, Johnson SW, and Canavier CC. A modeling study suggests complementary roles for GABAA and NMDA receptors and the SK channel in regulating the firing pattern in midbrain dopamine neurons. *J Neurophysiol* 91: 346-357, 2004.

Kopell N, Abbott LF, and Soto-Trevino C. On the behavior of a neural oscillator electrically coupled to a bistable element. *Physica D* 121: 367-395, 1998.

Landisman CE, Long MA, Beierlein M, Deans MR, Paul DL, and Connors BW. Electrical synapses in the thalamic reticular nucleus. *J Neurosci* 22: 1002-1009, 2002.

Manor Y, Rinzel J, Segev I, and Yarom Y. Low-amplitude oscillations in the inferior olive: a model based on electrical coupling of neurons with heterogeneous channel densities. *J Neurophysiol* 77: 2736-2752, 1997.

Marder E and Eisen JS. Electrically coupled pacemaker neurons respond differently to same physiological inputs and neurotransmitters. *J Neurophysiol* 51: 1362-1374, 1984a.

Marder E and Eisen JS. Transmitter identification of pyloric neurons: electrically coupled neurons use different transmitters. *J Neurophysiol* 51: 1345-1361, 1984b.

Marder E, Hooper SL, and Siwicki KK. Modulatory action and distribution of the neuropeptide proctolin in the crustacean stomatogastric nervous system. *J Comp Neurol* 243: 454-467., 1986.

Medvedev GS and Kopell N. Synchronization and transient dynamics in the chains of electrically coupled Fitzhugh-Nagumo oscillators. *Siam J Appl Math* 61: 1762-1801, 2001.

Medvedev GS, Wilson CJ, Callaway JC, and Kopell N. Dendritic synchrony and transient dynamics in a coupled oscillator model of the dopaminergic neuron. *J Comput Neurosci* 15: 53-69, 2003.

Miller JP and Selverston AI. Mechanisms underlying pattern generation in lobster stomatogastric ganglion as determined by selective inactivation of identified neurons. II. Oscillatory properties of pyloric neurons. *J Neurophysiol* 48: 1378-1391, 1982.

Perez Velazquez JL and Carlen PL. Gap junctions, synchrony and seizures. *Trends Neurosci* 23: 68-74, 2000.

Raper JA. Nonimpulse-mediated synaptic transmission during the generation of a cyclic motor program. *Science* 205: 304-306, 1979.

Selverston AI and Miller JP. Mechanisms underlying pattern generation in lobster stomatogastric ganglion as determined by selective inactivation of identified neurons. I. Pyloric system. *J Neurophysiol* 44: 1102-1121, 1980.

Selverston AI, Russell DF, and Miller JP. The stomatogastric nervous system: structure and function of a small neural network. *Prog Neurobiol* 7: 215-290, 1976.

Sherman A and Rinzel J. Rhythmogenic effects of weak electrotonic coupling in neuronal models. *Proc Natl Acad Sci U S A* 89: 2471-2474, 1992.

Sigvardt KA and Mulloney B. Properties of synapses made by IVN command-interneurones in the stomatogastric ganglion of the spiny lobster Panulirus interruptus. *J Exp Biol* 97: 153-168, 1982.

Skinner FK, Zhang L, Velazquez JL, and Carlen PL. Bursting in inhibitory interneuronal networks: A role for gap-junctional coupling. *J Neurophysiol* 81: 1274-1283, 1999.

Swensen AM and Marder E. Multiple peptides converge to activate the same voltage-dependent current in a central pattern-generating circuit. *J Neurosci* 20: 6752-6759, 2000.

Turrigiano G, LeMasson G, and Marder E. Selective regulation of current densities underlies spontaneous changes in the activity of cultured neurons. *J Neurosci* 15: 3640-3652, 1995.

Wilson CJ and Callaway JC. Coupled oscillator model of the dopaminergic neuron of the substantia nigra. *J Neurophysiol* 83: 3084-3100, 2000.

Figure Legends

Figure 1. The activity of the AB and PD neurons in response to current injection with intact modulatory inputs to the STG. Gray background shows 0 current injection, + denotes positive current injection and – denotes negative current injection. ***A.*** Voltage traces of the biological (left) AB (red) and PD (blue) neurons show in-phase bursting oscillations that become faster with increasing current injection in the AB neuron. This behavior is mimicked by the model neurons (right). I_{ext} in nA from top: Biological, 5, 3, 0.5, 0, –8, –8.5; Model, 5, 1.1, 0.8, 0, –0.22, –0.3. Minimum V_m in mV from top: Biological AB, 36, –41, –49, –51, –85, –86; Biological PD, –41, –42, –45, –46, –53, –54; Model AB, –45.2, –47.5, –48, –53, –52.4, –51 ; Model PD, –46, –46.5, –48.1, –53, –52.4, –51. The model pacemaker has a frequency range of 0.22 to 1.7Hz. ***B.*** Voltage traces of the synaptically-isolated biological (left) and model (right) AB neurons show bursting oscillations that become faster and smaller in amplitude with injected current. I_{ext} in nA from top: Biological, 33, 12, 6, 0, –3, –5; Model: 8, 1.0, 0.3, 0, –0.19, –0.27. Minimum V_m of the AB neuron in mV from top: Biological, 27, –17, –36, –60, –66, –76; Model, –44.6, –51, –54.8, –58.4, –59.2, –52.75. The model AB neuron has a frequency range of 0.24 to 3.4 Hz. ***C.*** Voltage traces from the isolated biological (left) and model (right) PD neurons show tonic spiking activity that increases in frequency with current injection. I_{ext} in nA from top: Biological, 15, 0, –1; Model: 12, 0, –0.3. Minimum V_m of the AB neuron in mV from top: Biological, –27, –50, –53; Model, –44, –46.5, –53. In the model, current injection runs were started at 0 nA with subsequent steps of 0.1 or 0.2 nA that lasted 20 to 30 s up to 8 nA (in A), 1.5 nA (in B) or 12 nA (in C). The current was then reset to 0 nA and subsequently decreased to –0.3 nA in steps of –0.01 nA or –0.02 nA.

Figure 2. The activity of the AB and PD neurons in response to current injection in the AB neuron in the absence of modulatory input. The biological AB (red) and PD (blue) neurons are quiescent with no current injections (gray background; left traces). Positive DC current injection (+) in the biological AB neuron evokes in-phase bursting oscillations that become faster with increasing current levels (left). This behavior is

reproduced by the model neurons (right). I_{ext} in nA from top: Biological, 10, 6, 1, 0; Model, 1, 0.6, 0.2, 0. Minimum V_m in mV from top: Biological AB neuron, −12, −35, −66, −77; Biological PD neuron, −51, −52, −55, −56; Model AB neuron, −45.3, −45.8, −48.2, −49.7; Model PD neuron, −47.7, −47.7, −48.5, −49.8. In the model, current injection runs were started at 0 nA, with subsequent steps of 0.2 nA up to 2 nA. Each run was 30 seconds.

Figure 3. The membrane potential waveform of the AB neuron is changed by electrical coupling to the PD neuron. **A.** Intracellular recordings show the waveforms of an AB neuron when electrically coupled (thin trace) to the PD neuron and when isolated (thick trace). Upon isolation, the average spike amplitude increased and the average spike number per burst decreased. Minimum V_m in mV: –61.3 mV for coupled and –62.9 mV for isolated AB neuron. **B.** A comparison of the waveforms in the model AB neuron when it is coupled to the PD neuron (thin trace) and when isolated (thick trace) shows that the isolated AB neuron waveform has a larger amplitude and shorter period, as in the biological neuron. The spike number per burst also decreased. Minimum V_m in mV: –53.5 mV for coupled and –58.4 mV for isolated AB neuron.

Figure 4. Compartmentalization of the model neurons. **A**. Schematic representation of the distribution of intrinsic currents in the model neurons. Ionic currents responsible for action potential generation were placed in the "A" (axon) compartment. Ionic currents underlying the generation of slow oscillations were placed in the S/N (soma-primary neurite) compartment. The presence of anterior inputs was modeled with a voltage-gated inward current I_{proc} in the model AB neuron, and with larger calcium currents I_{CaS} and I_{CaT} in the model PD neuron. In **B, C, D,** the top voltage traces correspond to the AB neuron and the bottom voltage traces to the PD neuron; the left traces show the membrane potential of the S/N compartments while those on the right show the A compartments. **B.** Activity of each compartment is shown in isolation, with parameters as described in Table 2. The lowest voltage values are for the AB neuron: −63.5 mV (S/N), −60 mV (A); for the PD neuron: −73 mV (S/N), −57.5 mV (A). **C.** Each S/N compartment shown in B is joined to the corresponding A compartment, with axial

conductances as in Table 2. The resulting input resistances were 14.8 MΩ (AB) and 6.9 MΩ (PD). The lowest voltage values are for the AB neuron: –58.4 mV (S/N), –74 mV (A); for the PD neuron: –46.5 mV (S/N), –72.5 mV (A). **D.** The two S/N compartments shown in C are electrically coupled to simulate a gap-junction with maximal conductance as in Table 2. The two model neurons now burst in-phase. The lowest voltage values are for the AB neuron: –53.5 mV (S/N), –74 mV (A); for the PD neuron: –53.5 mV (S/N), –73 mV (A).

Figure 5. The effects of varying the axial and gap-junctional conductances. The gray boxes show the activity of the "reference" model. **A.** Behavior of the S/N compartment of the isolated model AB neuron as the axial coupling between the S/N and A compartments is increased. The values (in μS) shown to the right are the maximal conductance of the axial current. The most hyperpolarized voltages in each trace are, from top (in mV): –61, –58.5, –58.4, –59.5 and –69. **B.** Behavior of the S/N compartment of the isolated model PD neuron as the axial coupling between the S/N and A compartments is increased. The values (in μS) shown to the right are the maximal conductance of the axial current; note that there is bistability at 0.8 μS. There was no change in the behavior of the neurons when couplings larger than the ones shown were used. The most hyperpolarized voltages are (from top to bottom in mV): –71, –67.8, –46, –46.5, –48.5, –52, –55 and –64. **C.** Behavior of the pacemaker AB-PD network as the gap-junctional conductance is increased. The red traces correspond to the AB neuron, the blue ones to the PD neuron. The traces are superimposed on the right to allow a direct comparison of the waveforms. The values (in μS) shown to the right are the gap junction conductances. The most hyperpolarized voltages are (from top to bottom in mV): –52.6, –54.7, –53.5, –57 and –58.

Figure 6. Comparison of the behavior of different AB-PD networks constructed from one- and two-compartment model neurons. **A.** Each column shows examples of outputs from a given network as the maximal conductance of the gap-junction is increased from top to bottom. Red voltage traces correspond to the model AB neuron and blue to the model PD neuron. The diagram on top of each column describes the type of model

neuron used. Two-compartment models are shown with a thin line connecting the S/N and A compartments; one-compartment model neurons are shown with whole region between the two compartments shaded. Each of the two columns in Cases I though IV is built with the same AB neuron but two different PD neurons. The gray box shows the activity of the "reference" AB-PD network. The isolated neurons differ from the maximal conductances shown in Table 2 as follows. Case I AB: no difference; Case II AB g_{CaT} = 42 μS and g_{axial} = 100 μS; Case III AB: g_{axial} = 100 μS; Case IV AB: no difference. Cases I, II and III model PD neurons: g_{Na} = 2500 μS in the A compartment and g_{axial} = 100 μS. Cases I, II and III model PD neurons: g_{Na} = 2500 μS in the A compartment, g_{KCa} = 0 and g_{axial} = 500 μS. Case IV PD: no difference; Case IV PD: g_{KCa} = 0. The values for the gap-junction conductances are (from top in μS): Case I AB-PD: 0, 0.4, 1.0, 1.6, 100. Case I AB-PD: 0, 0.1, 1.6, 2, 100. Case II AB-PD: 0, 0.2, 0.75, 3, 100. Case II AB-PD: 0, 0.2, 1.5, 3, 100. Case III AB-PD: 0.4, 1.2, 2,100. Case III AB-PD: 0, 0.2, 0.8, 1.5, 100. Case IV: 0, 0.1, 0.75, 3, 100. The most hyperpolarized voltage values for the traces are (from top in mV). Case I AB-PD, AB: –58.2, –51, –52, –53,–69; PD: –71.2, –71,–70, –68,–69. Case I AB-PD, AB: –58.2, –50.2, –54.5, –68, –62.7, –68; PD: –73, –73, –70, –73.2, –68. Case II AB-PD, AB: –58.4,–45.8, –49.4, –63.6, –69; PD: –71.2, –71.2, –70,–71.5, –69. Case II AB-PD, AB: –58.4, –46.4,–51.6, –63.2, –69; PD: –72, –71.8, –69, –71,–69. Case III AB-PD, AB: –68, –51.6, –53.5, –65.2, –68.8; PD: –71.2, –71, –69.4, –72,–68.8. Case III AB–PD, AB: –68, –58.2, –49.2, –65.5, –68.8; PD: –72, –71.5, –70, –71.2, – 68.8. Case IV AB-PD, AB: –58.2, –54.5, –52.9, –53.7, –59.9; PD: –71.2, –51.2, –53, –56.7, –59.9. Case IV AB-PD, AB: –58.2, –49.8, –51.5, –55.8, –59.5; PD: –72, –47, –51.6, –55.8, –59.5. **B, C.** The ratio of the AB neuron burst amplitude when coupled to the PD neuron to the burst amplitude of the isolated AB neuron shown as a function of the maximal gap junction conductance. A zero ratio corresponds to a coupled AB neuron that produces tonic spikes instead of bursting oscillations. **B**. Plots of the burst amplitude ratios are shown for both the AB-PD network (**B**) and the AB-PD network (**C**) in Cases I to IV.

Figure 7. The oscillation period range of a model AB-AB network and the model AB-PD network as a function of the gap-junction strength (in μS). The burst period range was

obtained by DC current injection in the AB neuron (**A,B**) or the PD neuron (**C**), as depicted in the inset schematic network diagrams. The dashed curve represents no current injection; the top curve corresponds to the longest possible period that the network produced with hyperpolarizing current injection before becoming quiescent; the bottom curve represents the shortest period that the network produced with depolarizing current injection before the bursts became irregular or changed to tonic spiking. The gray area shows the burst period range of the isolated AB neuron. The white insets show 2 s long voltage traces of the coupled neurons for a coupling conductance of 0.01 μS and the largest hyperpolarizing current injection. The voltage in the insets is from –60 mV to –30 mV. **A.** An AB-AB model network cannot oscillate with periods longer than those of an isolated AB model neuron. For small coupling conductances (< 0.3 μS) its period range was smaller than that of the isolated AB neuron. The inset shows two phase-locked AB neurons when hyperpolarizing current (I = –0.41 nA) was applied to one of them (lighter traces). **B**. When current is injected into the model AB neuron, for small to moderate coupling conductance the AB-PD network can produce slower (but not faster) oscillations than the isolated AB neuron. The inset shows phase-locked bursting with the PD neuron bursting slightly earlier, as hyperpolarizing current (I = –0.23nA) was injected into the AB neuron. **C**. When current is injected into the model PD neuron, the AB-PD network period range of oscillations is smaller than that of the isolated AB. The inset shows phase-locked bursting, with the AB neuron bursting slightly earlier, as hyperpolarizing current (I = –0.27nA) was injected into the PD neuron. The most hyperpolarized voltages in the insets are (in mV): –56.5 (**A**), –48.2 (**B**) and –52.2 (**C**).

Figure 8. The currents that participate in the ~1 Hz oscillations in the isolated S/N compartments, and their behavior in the isolated model neuron. For each model neuron, the leftmost column shows the currents for its isolated S/N compartment, and the rightmost column shows the same currents when the S/N and A compartments are connected. The boxes in the first three columns display the currents at a different scale for 600 ms duration, after the first 100 ms of activity. The boxes in the fourth column display enlargements of the full 1100 ms of activity. Parameters are as in Table 2.

Figure 9. Currents in the S/N compartments of the AB-PD pacemaker model network in the presence of modulatory inputs. The boxes show enlargements of 600 ms of activity.

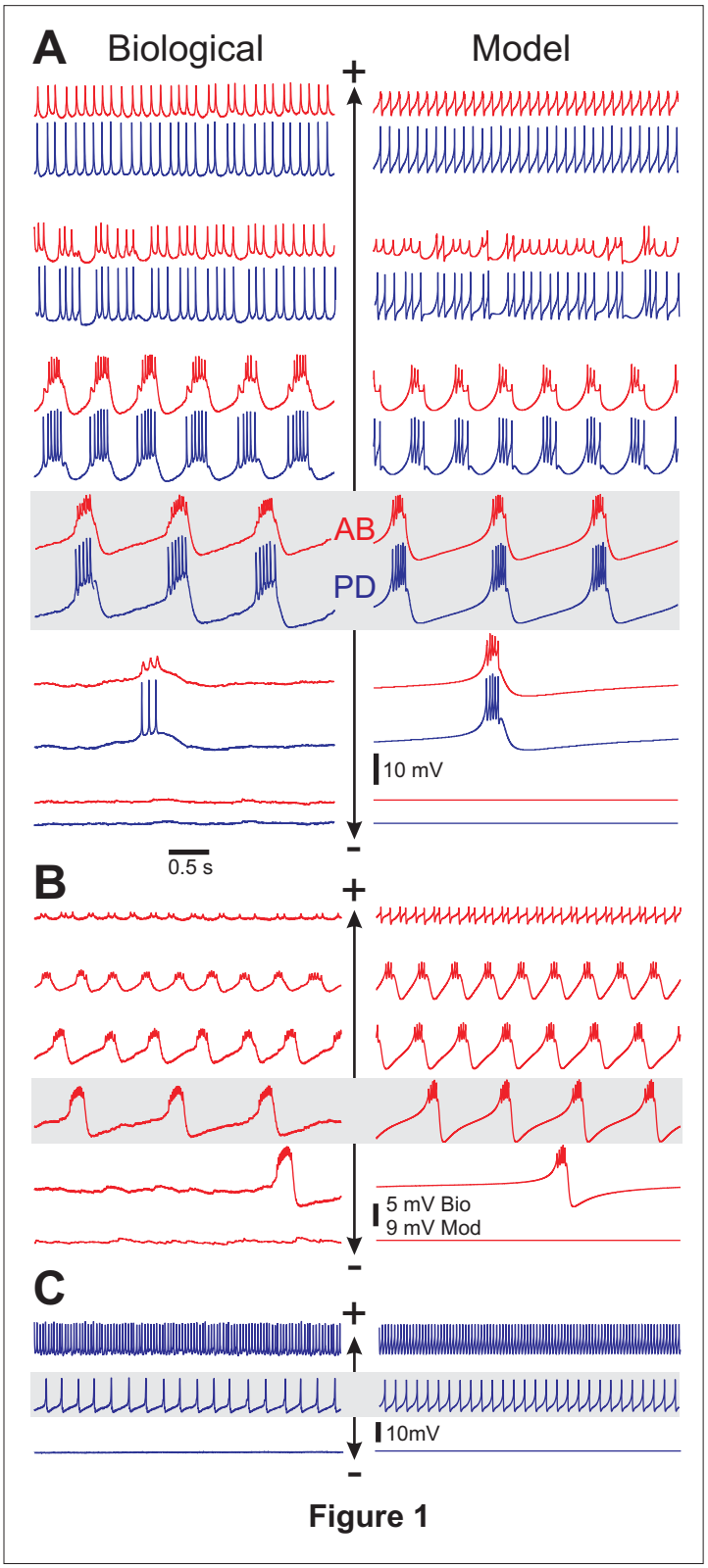

Figure 1

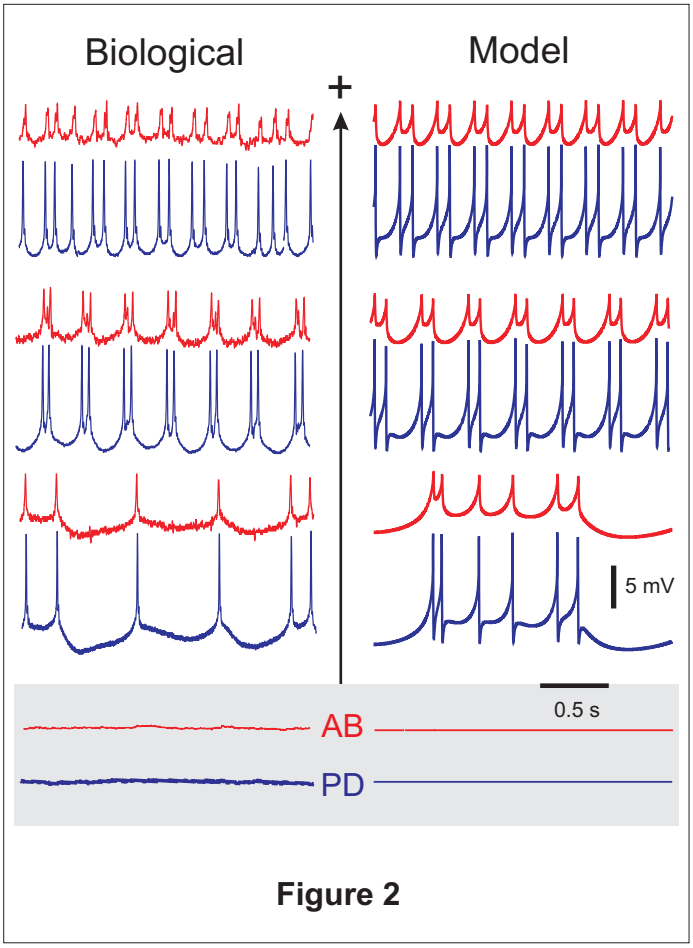

Figure 2

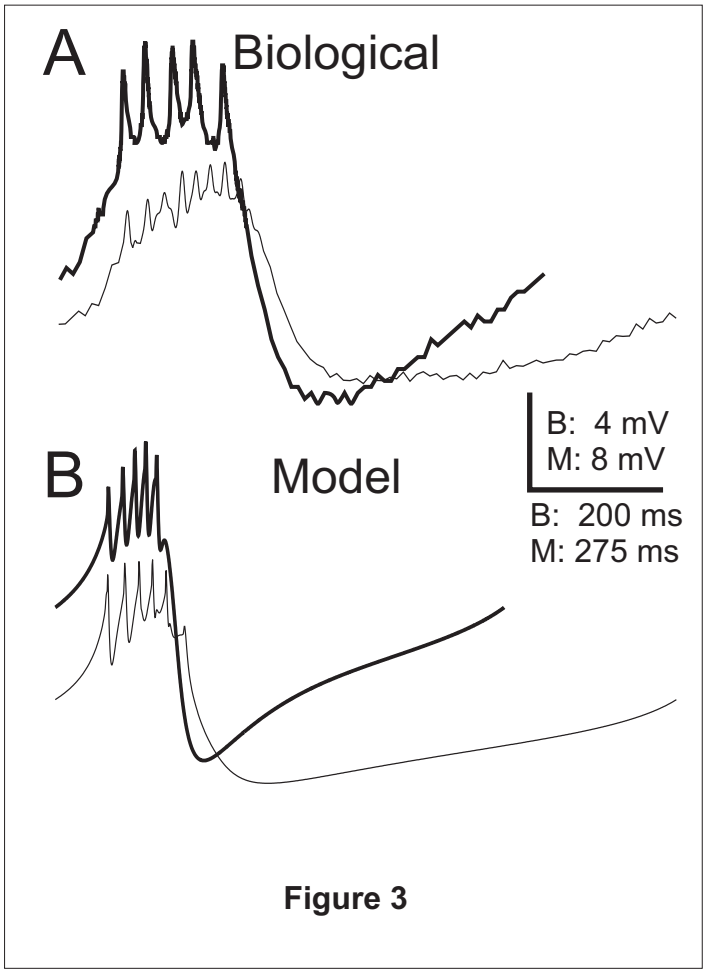

Figure 3

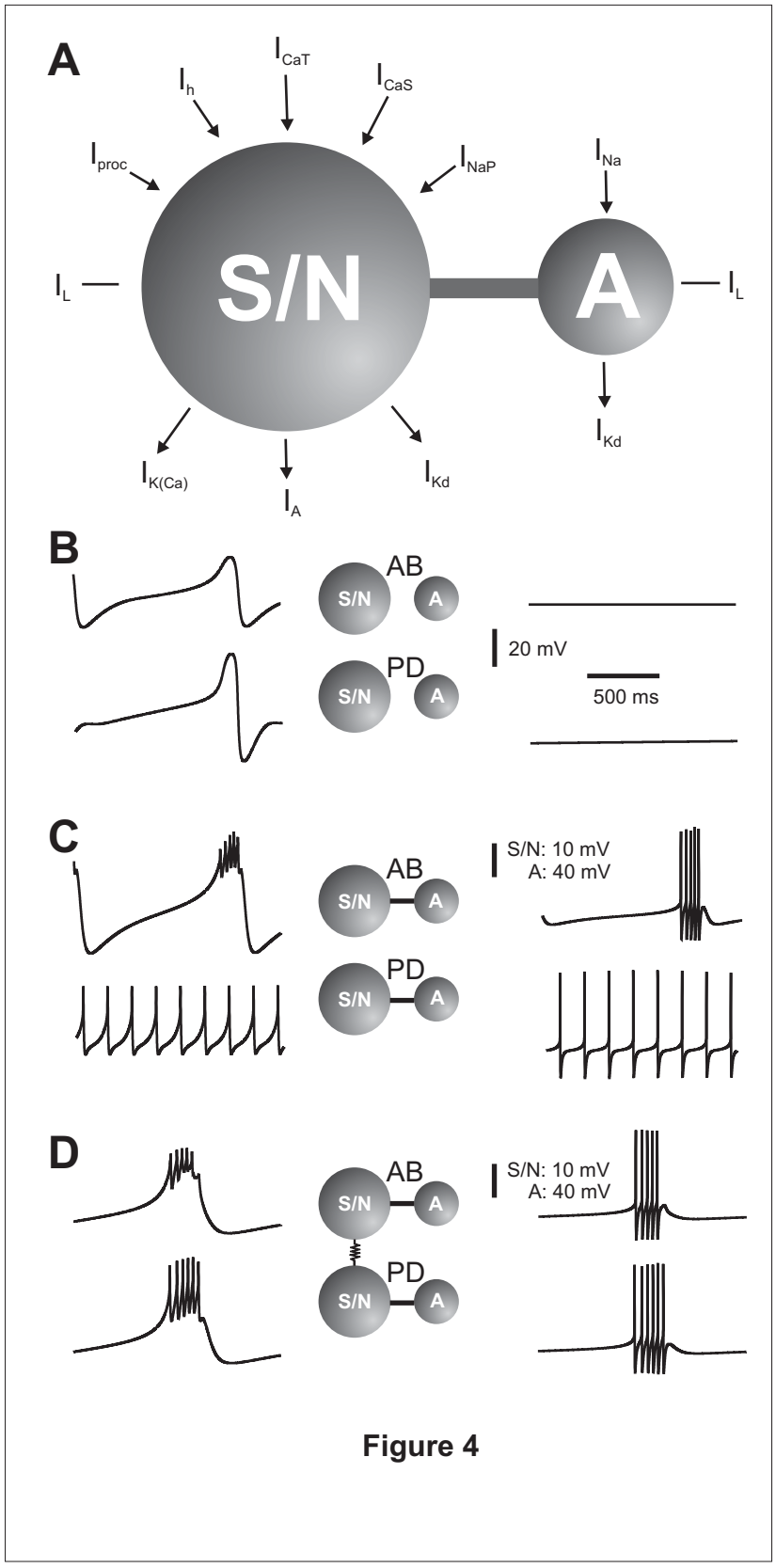

Figure 4

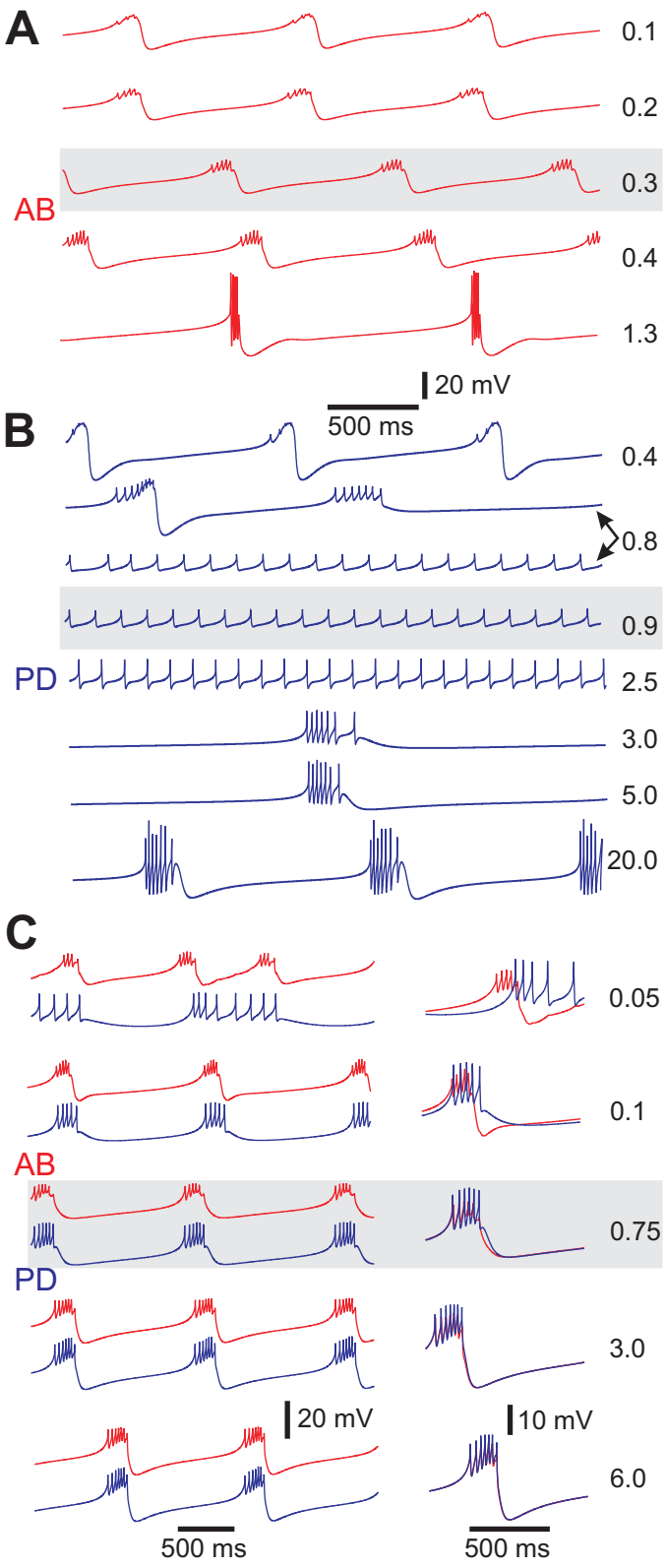
A
0.1
0.2
AB
0.3
0.4
1.3
20 mV
500 ms
B
0.4
0.8
0.9
PD
2.5
3.0
5.0
20.0
C
0.05
0.1
AB
0.75
PD
3.0
20 mV
10 mV
6.0
500 ms
500 ms

Figure 5

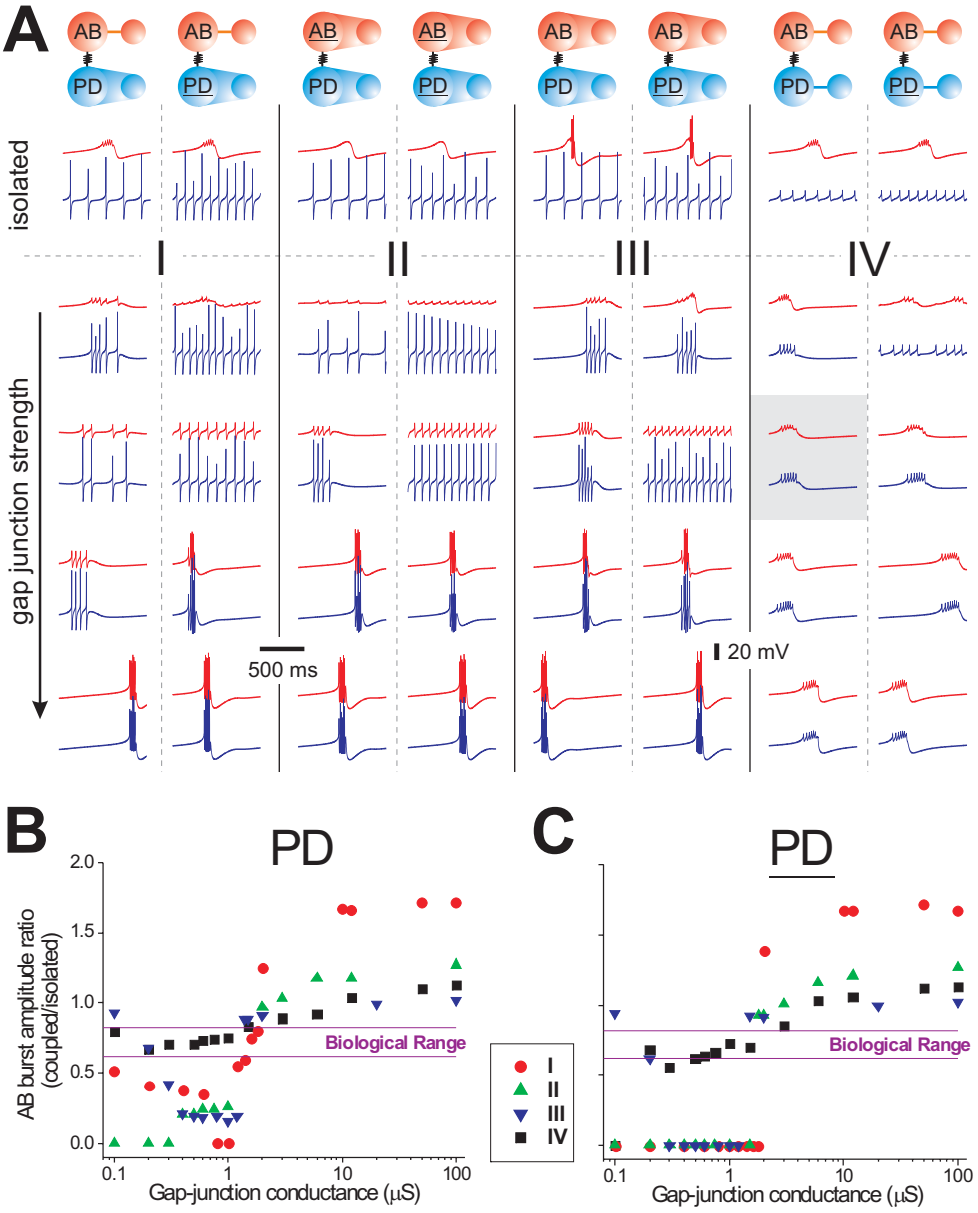
A
AB
PD
isolated
I
II
III
IV
gap junction strength
500 ms
20 mV
B
PD
AB burst amplitude ratio (coupled/isolated)
2.0
1.5
1.0
0.5
0.0
Biological Range
0.1
1
10
100
Gap-junction conductance (µS)
I
II
III
IV
C
PD
Biological Range
0.1
1
10
100
Gap-junction conductance (µS)

Figure 6

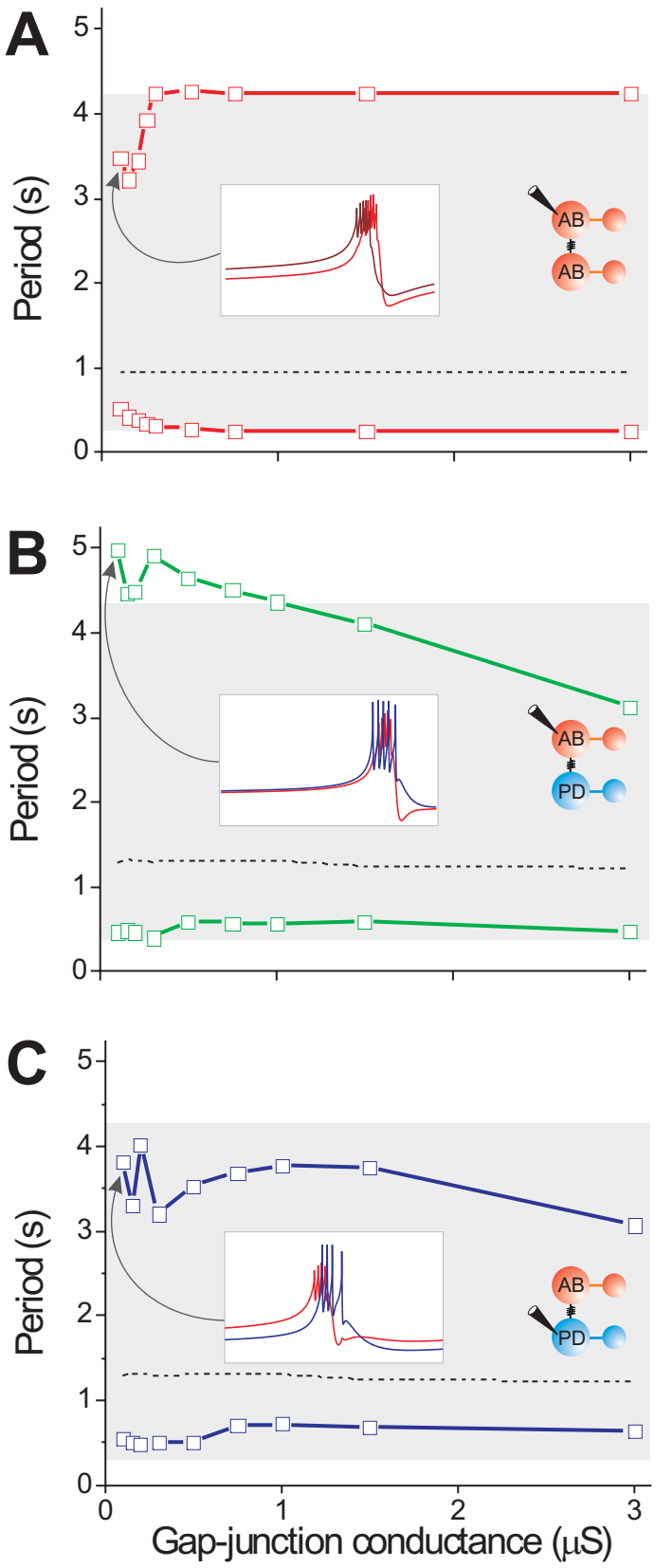

Figure 7

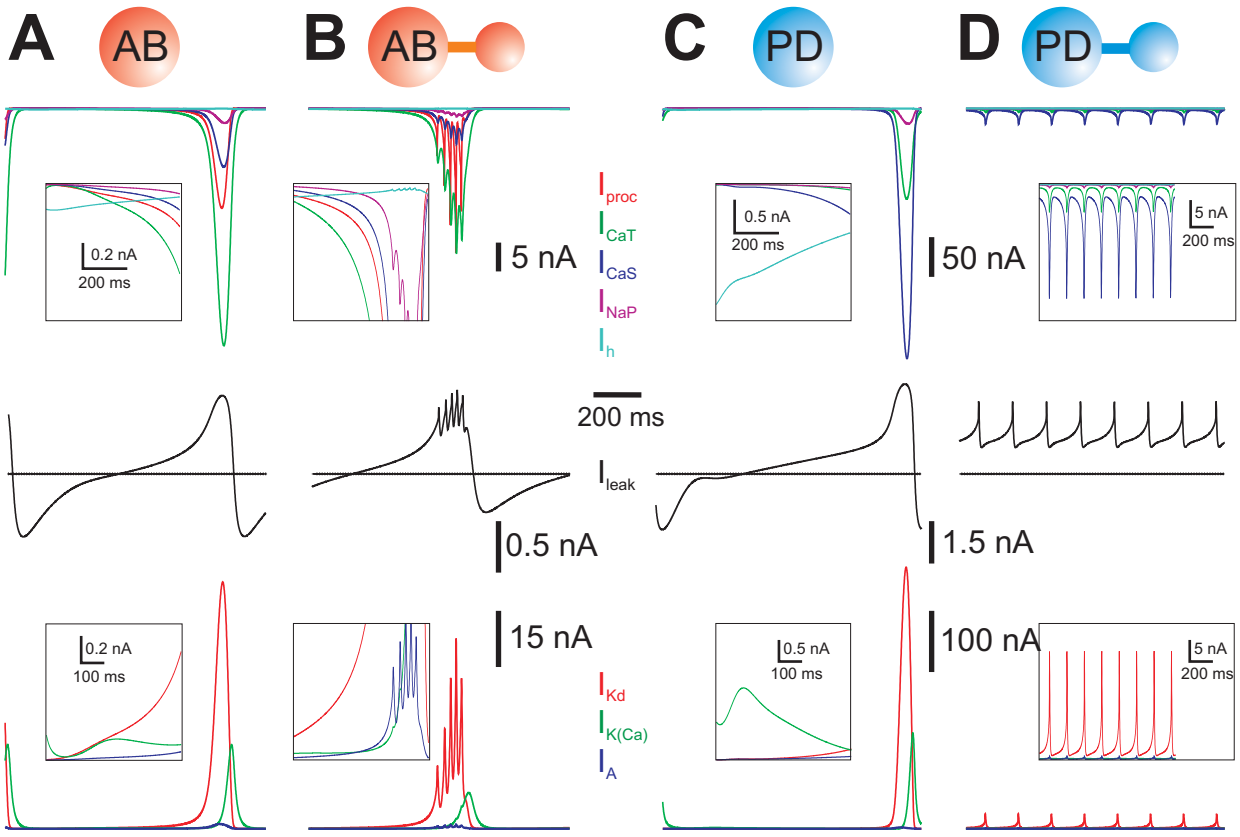
A
AB
B
AB
C
PD
D
PD
0.2 nA
200 ms
5 nA
0.5 nA
200 ms
50 nA
5 nA
200 ms
I proc
I CaT
I CaS
I NaP
I h
200 ms
I leak
0.5 nA
1.5 nA
0.2 nA
100 ms
15 nA
0.5 nA
100 ms
100 nA
5 nA
200 ms
I Kd
I K(Ca)
I A

Figure 8

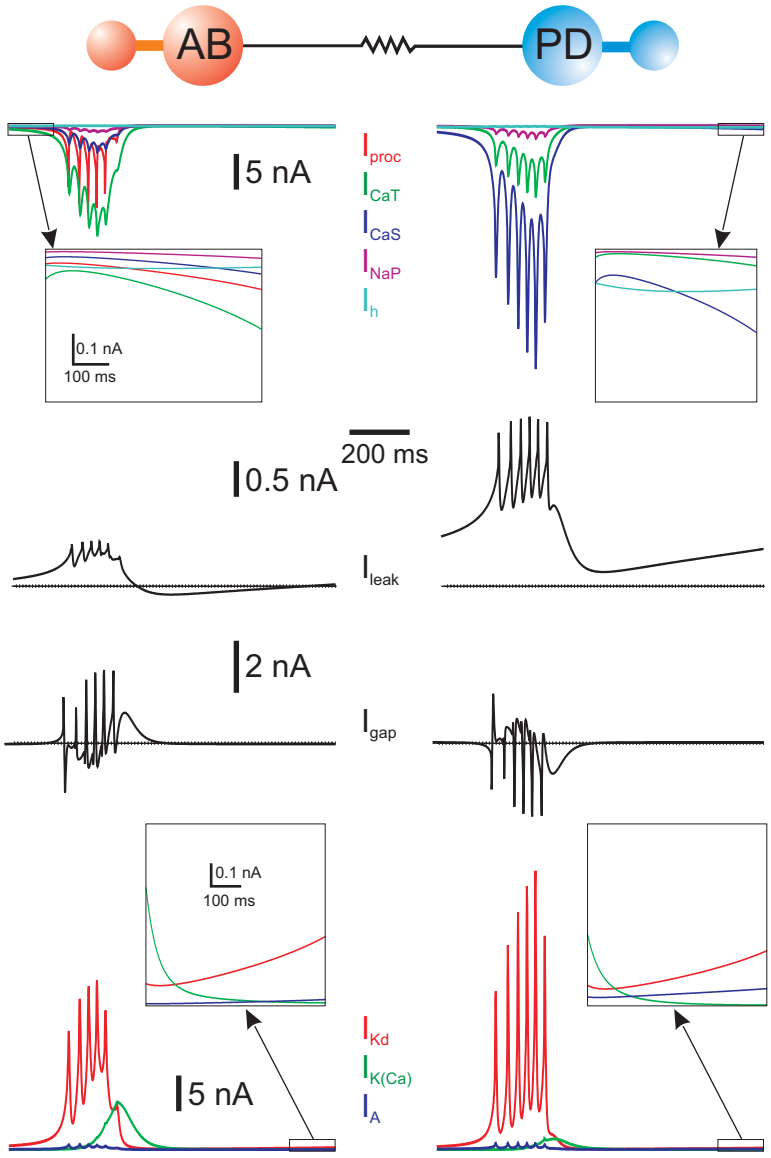
AB
PD
5 nA
0.1 nA
100 ms
I proc
I CaT
I CaS
I NaP
I h
200 ms
0.5 nA
I leak
2 nA
I gap
0.1 nA
100 ms
5 nA
I Kd
I K(Ca)
I A

Figure 9